

Formation Flight Design Near Earth-Moon Lagrange Points for Interferometric Characterization of Cislunar Objects

Erin E. Fowler and Derek A. Paley

Department of Aerospace Engineering, University of Maryland College Park

ABSTRACT

The cislunar regime is of increasing interest to the space industry due to its value for applications such as astronomy, interplanetary mission staging, lunar exploration and communications, and Earth orbit insertion. The research described here is specific to the Earth-Moon system and determines advantageous formations for interferometric imaging of other spacecraft in the cislunar regime for space domain awareness and spacecraft characterization applications based on metrics for imaging and object tracking as well as an instability metric to approximate the control cost for the proposed formation. Previous research related to this topic describes a continuous feedback control algorithm that maintains a formation of satellites in motion that is bounded relative to a halo orbit in the Sun-Earth/Moon system and shows image reconstruction and (u, v) plane coverage for interferometric satellite configurations for astronomy applications [7].

1. INTRODUCTION

The National Cislunar Science & Technology Strategy published by the White House Office of Science & Technology Policy in November 2022 states: “The United States should advance Cislunar [space situational awareness (SSA)] by initially identifying an architecture that optimizes terrestrial, Lunar-based, and space-based sensors, then leveraging existing ground-based sensors and developing new ground-based sensors as needed... In-space tests should leverage orbits available in Cislunar space that can potentially enhance SSA capabilities.”[2] The Cislunar Security National Technical Vision published by the Johns Hopkins Applied Physics Laboratory in November 2022 states: “Challenges to cislunar SSA include the need for highly accurate object observations at large distances and through obscuration, exclusion zones, and periods when the target object may be unlit (via various sensor phenomenologies); sufficiently detailed dynamic modeling (maintaining nonlinearities); and appropriate algorithms (filters) for combining expectation with observation and incorporating domain knowledge to produce successful predictions of future object states. Tracking cislunar objects will require a paradigm change when compared to tracking objects in lower Earth orbits.”[15]

Objects near the Moon are approximately ten times farther from the Earth than the farthest objects being tracked in traditional space domain awareness efforts, i.e., objects in geosynchronous Earth orbits. Due to these large distances, new space-based sensing strategies must be considered for cislunar space domain awareness and particularly for spacecraft characterization, which may require better resolution than any single optical telescope can offer, including exquisite and expensive sensors like the Hubble Space Telescope. Interferometric sensing strategies using multiple smaller and less expensive sensors promise resolution equivalent to what could be produced by a single telescope the size of the largest baseline, or distance between sensors, in the spatial direction of that baseline.

Relative motion control has never been attempted near Earth-Moon Lagrange points, and a formation flight design for interferometric imaging of resident space objects in the cislunar regime would enable novel and highly capable sensing at large distances for cislunar space domain awareness and other missions. Trajectories in three-body dynamics must be identified numerically because no comprehensive analytical solution exists for the three-body equations of motion, whereas analytical solutions to the two-body equations of motion do exist and are used in the development of rendezvous algorithms. Although dynamics become nearly linear when satellites are in close proximity in Earth orbit, even at these close distances the dynamics near Lagrange points remain highly nonlinear, requiring a departure from two-body relative motion models and two-body algorithms for proximity operations. Algorithms like the well-known Hill-Clohessy-Wiltshire equations for two-body relative dynamics can be used to control relative motion in most Earth orbits, but solutions for relative motion in three-body dynamics are very specific to the chosen reference orbit (where

options can include Lyapunov orbits in the plane of the Moon’s orbit about the Earth, Lissajous quasi-periodic orbits, halo orbits, distant retrograde orbits, and others).

Significant previous research has been published on the topic of formation flying in two-body Keplerian dynamics and specifically Earth orbits, but research on the topic of formation flying near Lagrange points in three-body systems is more limited. Previous research related to the topic of formation flight near Lagrange points includes [7] and [12], which show image reconstruction and (u, v) plane coverage for interferometric satellite configurations for astronomy applications and describe a continuous feedback control algorithm that maintains a formation of satellites in motion that is bounded relative to a halo orbit in the Sun-Earth/Moon system. The research described in this manuscript is specific to the Earth-Moon system and determines advantageous formations for interferometric imaging of other spacecraft in the cislunar regime for space domain awareness, tracking, and spacecraft characterization applications based on a metric for coverage of the (u, v) plane, a geometric plane defined for the analysis and processing of interferometric observations, as well as a tracking custody metric and an instability metric to approximate the control cost for the proposed formation.

In order to study high-performing satellite formations for the purpose of interferometric characterization of cislunar objects, we begin by choosing initial conditions and propagating trajectories for a satellite formation about a reference Lyapunov (in-plane) orbit about Earth-Moon Lagrange point L2, as well as choosing initial conditions and propagating a trajectory for a target object in an in-plane orbit about Earth-Moon Lagrange point L4. We then develop algorithms for transforming these relative motions into the (u, v) plane and plotting those results. We then produce a metric for (u, v) plane coverage to aid in the choice of the initial conditions of the interferometer formation. We compare the results for this metric to the tracking custody that can be maintained with the simulated interferometric measurements, and we show the trade of improvements in resolution and tracking custody against the increased control effort required to maintain the formation, according to our control effort approximation.

The contributions of this paper are (1) a metric for (u, v) plane coverage for an interferometer collecting astrometric measurements from cislunar space against objects elsewhere in cislunar space, (2) a metric for tracking custody that uses the resolution of the simulated interferometer in a batch least squares estimator and propagates the resulting estimated target object state, (3) a metric which approximates the control effort required to maintain the formation, and (4) analysis of the performance of a series of formations of 4–16 satellites about a reference Earth-Moon L2 orbit against the (u, v) plane coverage, custody, and control effort metrics.

The organization of this paper is as follows. Section 2 introduces the Circular Restricted Three-Body Problem (CR3BP), the simplified dynamic system in which the cislunar trajectories studied in this research are developed, and interferometry as a measurement method, including the van Cittert-Zernike theorem which provides the basis for this measurement method and defines the (u, v) plane. Section 3 describes the methodology used in this research, which aims to develop metrics to optimize observer spacecraft formations near Earth-Moon Lagrange points enabling interferometric imaging of distant spacecraft in the cislunar system, for the ultimate goal of cislunar space domain awareness and tracking. Section 4 shows (u, v) plane coverage, tracking custody, and control effort results for various observer formations about Earth-Moon Lagrange point L2, observing a spacecraft which orbits L4. Section 5 describes concepts for future work and extensions of this research.

2. BACKGROUND

The goal of this research is to assess the value of various formations near a Lagrange point in the Earth-Moon system (cislunar space) for the application of interferometric collections against another object in cislunar space, based both on the contribution that the interferometric measurements made by the formation can be expected to add to a cislunar object tracking capability and on the control effort that may be required to maintain the formation of satellites on their desired relative trajectories. The resolution of the measurement produced by an interferometric satellite array is largely determined by the corresponding coverage of the (u, v) plane, which is derived based on the motion of the satellites in physical space [7]. Concepts that underpin this research thus include cislunar dynamics and relative motion in the Circular Restricted Three-Body Problem as well as interferometry as a measurement method.

2.1 Relative Motion in the Circular Restricted Three-Body Problem

Motion within the Earth-Moon system may be approximated using the dynamics of the Circular Restricted Three-Body Problem (CR3BP), in which the motion of a spacecraft with negligible mass is modeled under the influence of

the gravitation of two primaries approximated as point masses in circular orbits about their barycenter [10]. A solution in the CR3BP can be one of four types [4]: an equilibrium point, a periodic orbit (Lyapunov or halo), a quasi-periodic orbit (Lissajous), and chaotic motion.

At equilibrium points in the CR3BP (known as Lagrange or libration points), gravitational forces and rotational accelerations are balanced [16]. At stable equilibrium points (Earth-Moon L4 and L5), perturbations cause oscillations about the equilibrium point, whereas at unstable equilibrium points (Earth-Moon L1, L2, L3), perturbations cause drift away from the equilibrium point. However, if initial conditions are restricted such that only the non-divergent mode is allowed, the coupled motion in the xy plane is bounded and periodic about these collinear Lagrange points [10]. The planar periodic orbits surrounding L1, L2, and L3 are called Lyapunov orbits, and their three-dimensional counterparts are called halo and Lissajous orbits [10]. For the purpose of this research, periodic trajectories are generated according to [5]. For further discussion of the dynamics of the CR3BP, see [3].

Relative motion control has never been attempted near Earth-Moon Lagrange points, and a formation flight design for interferometric imaging of resident space objects in the cislunar regime would enable novel and highly capable sensing at large distances for cislunar space domain awareness and other missions. Suppose that two spacecraft exist near Earth-Moon Lagrange point L2 and have initial conditions chosen to avoid exciting the divergent mode of the linearized equations of motion about the collinear Lagrange point. In other words, for the linearized equations of motion, a solution to the equations can be made to contain only the oscillatory modes with the following choice of initial conditions [17]:

$$\begin{aligned} \dot{x}(0) &= \left(\frac{\omega_{xy}}{k}\right)y(0) \\ \dot{y}(0) &= -k\omega_{xy}x(0), \end{aligned} \quad (1)$$

where $k = \frac{\omega_{xy}^2 + U_{XX}}{2\omega_{xy}\omega}$ is a non-oscillatory poles-nulling factor, ω_{xy} is the nondimensional frequency of the in-plane oscillatory mode, and ω_z is the nondimensional frequency of the out-of-plane oscillatory mode. Values for k , ω_{xy} , and ω_z are calculated as follows:

$$\begin{aligned} \omega_{xy} &= \sqrt{\beta_1 + \sqrt{\beta_1^2 + \beta_2^2}} \\ \beta_1 &= 2\omega^2 - (U_{XX} + U_{YY})/2 \\ \beta_2^2 &= -U_{XX}U_{YY} \\ \omega_z &= \sqrt{|U_{zz}|} \end{aligned} \quad (2)$$

The parameter U with a double-lettered subscript indicates the second derivative of pseudopotential U with respect to that lettered variable, i.e.,:

$$\begin{aligned} U_{XX}|_{L_2} &= \omega^2 + \frac{2Gm_1}{(x_{L2} + r_1)^3} + \frac{2Gm_2}{(x_{L2} - r_2)^3} \\ U_{YY}|_{L_2} &= \omega^2 - \frac{Gm_1}{(x_{L2} + r_1)^3} - \frac{Gm_2}{(x_{L2} - r_2)^3} \\ U_{ZZ}|_{L_2} &= -\frac{Gm_1}{(x_{L2} + r_1)^3} - \frac{Gm_2}{(x_{L2} - r_2)^3} \end{aligned} \quad (3)$$

Out-of-plane initial conditions are arbitrary because out-of-plane motion is oscillatory. Equation (1) does not produce initial conditions that avoid exciting the divergent mode if higher-order terms in U are retained, but these initial conditions suffice for initial formation design, particularly when initial conditions are close to the Lagrange point [17]. Note the error discovered in the β_1 equation and corrected here in Equation (2): the ω term is not squared in [6] and is missing from this equation in [17].

With the initial conditions described above, the solution to the linearized equations of motion is [17]:

$$\mathbf{r}(t) = \begin{bmatrix} x(t) \\ y(t) \\ z(t) \end{bmatrix} = \begin{bmatrix} x_0 \cos(\omega_{xy}(t-t_0)) + \frac{y_0}{k} \sin(\omega_{xy}(t-t_0)) \\ -kx_0 \sin(\omega_{xy}(t-t_0)) + y_0 \cos(\omega_{xy}(t-t_0)) \\ z_0 \cos(\omega_z(t-t_0)) + \frac{\dot{z}_0}{\omega_z} \sin(\omega_z(t-t_0)) \end{bmatrix} \quad (4)$$

Subscript 0 refers to a value at time $t = t_0$, and can be rewritten as a pair of decoupled matrix equations of similar form [17]:

$$\begin{bmatrix} x \\ y \end{bmatrix} = \begin{bmatrix} \cos(\omega_{xy}(t-t_0)) & \frac{1}{k} \sin(\omega_{xy}(t-t_0)) \\ -k \sin(\omega_{xy}(t-t_0)) & \cos(\omega_{xy}(t-t_0)) \end{bmatrix} \begin{bmatrix} x_0 \\ y_0 \end{bmatrix} \quad (5)$$

$$\begin{bmatrix} z \\ \dot{z} \end{bmatrix} = \begin{bmatrix} \cos(\omega_z(t-t_0)) & \frac{1}{\omega_z} \sin(\omega_z(t-t_0)) \\ -\omega_z \sin(\omega_z(t-t_0)) & \cos(\omega_z(t-t_0)) \end{bmatrix} \begin{bmatrix} z_0 \\ \dot{z}_0 \end{bmatrix}$$

By comparing Equation (5) as t evolves, relative motion equations can be found as follows [17]:

$$\begin{bmatrix} \Delta x \\ \Delta y \end{bmatrix} = \begin{bmatrix} \cos(\omega_{xy}(t-t_0)) & \frac{1}{k} \sin(\omega_{xy}(t-t_0)) \\ -k \sin(\omega_{xy}(t-t_0)) & \cos(\omega_{xy}(t-t_0)) \end{bmatrix} \begin{bmatrix} \Delta x_0 \\ \Delta y_0 \end{bmatrix} \quad (6)$$

$$\begin{bmatrix} \Delta z \\ \Delta \dot{z} \end{bmatrix} = \begin{bmatrix} \cos(\omega_z(t-t_0)) & \frac{1}{\omega} \sin(\omega_z(t-t_0)) \\ -\omega_z \sin(\omega_z(t-t_0)) & \cos(\omega_z(t-t_0)) \end{bmatrix} \begin{bmatrix} \Delta z_0 \\ \Delta \dot{z}_0 \end{bmatrix}$$

Equation (6) produces elliptical motion with amplitude defined by the initial conditions Δx_0 , Δy_0 , Δz_0 and can thus be used to determine the initial conditions that will produce some desired relative motion between a pair of satellites over time. Since these equations reflect a linearized solution, they offer an aid to finding initial conditions but produce trajectories that ultimately diverge from both the CR3BP dynamic propagation and any higher-fidelity dynamic propagation over time. Thus in reality, control effort will be required to maintain a formation's motion along the desired solution obtained from these linearized results.

2.2 Interferometry

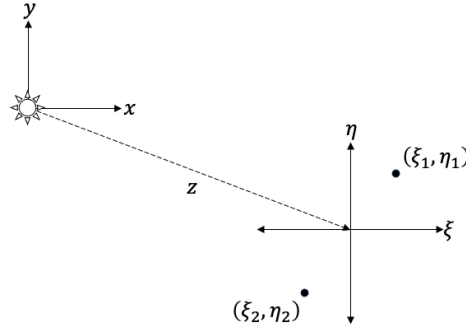


Fig. 1: A depiction of the architecture of an interferometric imaging system, inspired by a similar figure in [7]. The target object is emitting or reflecting light of frequency λ from the origin of the (x, y) plane. The formation is at distance z from the target. The positions of the satellites in the formation are projected into the (ξ, η) plane so that the spatial frequencies (points in the (u, v) plane) sampled by the interferometer can be calculated.

The van Cittert–Zernike theorem [21], named after physicists Pieter Hendrik van Cittert and Frits Zernike, is a formula that states that under certain conditions the Fourier transform of the intensity distribution function of a distant, incoherent source is equal to its complex visibility, providing the basis for interferometric imaging. The theorem implies that if the value of the complex mutual coherence function is known at every point in the (u, v) plane, a two-dimensional Fourier transform may be used to create an image [12]. The van Cittert-Zernike result provides an equation for the image of a source [7]:

$$I(x, y) \approx \int_u \int_v \mu(u, v) e^{i2\pi(ux+vy)} dv du, \quad (7)$$

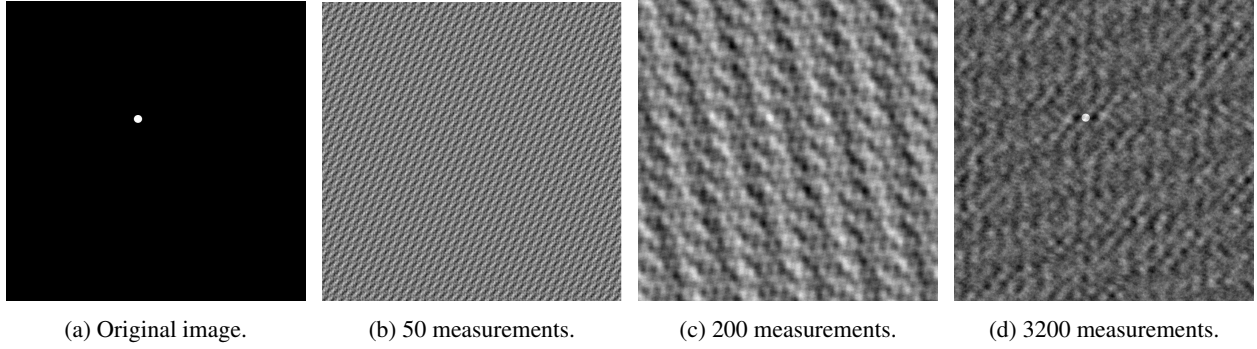


Fig. 2: Simulated interferometric reconstruction of an image of 800×800 pixels based on randomly selected points on the (u, v) plane.

where $\mu(u, v)$ is the complex mutual coherence function. The (u, v) plane, the plane of spatial frequencies sampled by an interferometer that are input to the mutual coherence function μ , is a function of the position of the interferometer, its baselines, the wavelength sampled by the interferometer, and the target coordinates. Depicted in Fig. 1, the (u, v) plane is defined by [7]

$$\begin{aligned} u &= \frac{\eta_1 - \eta_2}{z\lambda} \\ v &= \frac{\xi_1 - \xi_2}{z\lambda}, \end{aligned} \quad (8)$$

where λ represents the wavelength of light emitted or reflected by the target and collected by the interferometer. Based on Equation (8), it is clear that the image of the source depends on u and v , which depend on the locations of the satellites in (ξ, η) space. If all points in (u, v) space (all spatial frequencies) can be sampled, then the complete image can be reconstructed by the interferometer. In the case of an interferometer with two telescopes of diameter D and separated by a baseline vector \mathbf{B} defined in the (ξ, η) plane, the (u, v) plane consists of a low-frequency peak of extent $\pm D/\lambda$ and two high-frequency peaks of extent $\pm D/\lambda$ and located at $\pm \mathbf{B}/\lambda$ [14]. The interferometer acts thus as a high-frequency band pass filter, allowing it to reach information at a resolution of $1.22\lambda/|\mathbf{B}|$, outperforming a single telescope of diameter D with resolution $1.22\lambda/D$. An interferometer consisting of n telescopes produces $\frac{n(n-1)}{2}$ baselines and thus samples $\frac{n(n-1)}{2}$ frequencies in the Fourier transform of the brightness distribution of the object [14].

Given that the (u, v) plane coverage defines the sampling of the Fourier transform of the object brightness distribution, sparse sampling of the (u, v) plane is a common concern for interferometry as compared to single-dish observations. Sparse sampling results in lower signal-to-noise ratio (lower sensitivity). According to [1], “noise magnitude is inversely proportional to the square root of the collection area of the telescopes. Thus, the noise can be reduced by increasing the collection area of the telescopes. However, note that costs (and other possible issues such as fuel usage) often dictate the size of the telescopes that can be put in space.” Also introduced in [1] is the helpful notion of image formation by a multi-spacecraft interferometric imaging system being analogous to “‘painting’ of a big disk by a number of smaller ‘coverage disks’ or ‘paintbrushes’”, a notion which emphasizes the importance of (u, v) coverage for interferometers. Fig. 2, which shows an improving image reconstruction as a function of increasing numbers of randomly sampled (u, v) points against a digital original image, further exemplifies the importance of abundant sampling of the spatial frequencies in the (u, v) plane defined against a particular source. Because the interferometry application studied in this research is tracking a distant object in cislunar space, the details of that object need not be resolved, but the interferometer does need to sample enough spatial frequencies to precisely identify the angular location of the object on the celestial sphere as input to a state estimation algorithm used to track the object.

Interferometers can be optimized for various types of measurement, resulting in various (u, v) plane coverage metrics. For example, interferometers can be used for visibility measurements (detecting the size of an object), astrometry (detecting the position of an object), and imaging (detecting the structural details of an object). Long baselines measure information about the small-scale structure of the source but are insensitive to large-scale structure; conversely, short baselines measure information about the large-scale structure of the source but are insensitive to small-scale structure. In order to precisely measure the position of a target object (astrometry), baselines \mathbf{B} should be as long as possible

without actually resolving the target [13]. Thus, in order to optimize the placement of telescope elements in an interferometer for a particular type of measurement against a target, some characteristics of the target must be estimated in advance of the measurement.

For a multiple-element array, the best choice of spacing is to create uniform sampling of the (u, v) plane. The uniform sampling of spatial frequencies helps avoid degeneracies or aliasing in image reconstruction [19]. As the target and individual telescopes in the interferometer move due to natural or forced-motion dynamics, baseline length and orientation change, resulting in measurements over different spatial frequencies and directions, filling in the (u, v) plane for better image synthesis.

A specific description of space-based interferometry is provided by [8]: “Interferometric imaging is performed by measuring the mutual intensity ... that results from the collection and subsequent interference of two electric field measurements of a target made at two different observation points. While moving relative to each other, the satellites collect and transmit these measurements, which are later combined at a central node using precise knowledge of their locations and timing of data collection. A least squares error estimate of the image can be reconstructed given the mutual intensity measurements, parameters of the optical system, and the physical configuration of the observatory.” A benefit to flying a space-based optical long-baseline interferometer is that it removes the requirement for ground-based interferometers to rapidly and constantly monitor atmospheric effects, but an obstacle for a space-based free-flying interferometer performing direct detection (homodyne) interferometry is the requirement for extremely precise relative position control, within a wavelength of the sampled light [9][18]. According to [9], while less sensitive than direct detection interferometry, heterodyne interferometry allows this requirement for precise position *control* to be safely neglected in favor of precise position and timing *knowledge* among interferometer elements, allowing for the use of a “widely dispersed, loosely organized ‘swarm’ of functionally identical spacecraft-borne optics” to perform the desired mission based on the use of a “precise metrology system and large-scale, parallel signal processing to perform interferometric imaging without the requirement of precise inter-spacecraft positioning and alignment control.”

3. METHODOLOGY

In order to study the interferometric result that would be produced by a particular formation of satellites near Earth-Moon L2, we begin by choosing an epoch and initial conditions for a target orbiting Earth-Moon L4. The simulation begins at midnight UTC on October 15, 2022. Non-dimensionalized initial conditions for the target object in the Earth-Moon rotating frame with origin at the barycenter are: $x = 0.7274$, $y = \frac{\sqrt{3}}{2}$, $z = 0$, $\dot{x} = 0.1306$, $\dot{y} = -0.2562$, $\dot{z} = 0$, based on initial conditions provided by [5]. Fig. 3 shows the motion of the formation reference trajectory and of the target object for four days.

We then choose the initial conditions for a reference or “leader” orbit for the formation orbiting Earth-Moon L2. Non-dimensionalized initial conditions for the nominal EML2 orbit in the Earth-Moon rotating frame with origin at the barycenter are: $x = 1.2200$, $y = 0$, $z = 0$, $\dot{x} = 0$, $\dot{y} = -0.4275$, $\dot{z} = 0$, based on initial conditions provided by [5].

To analyze the (u, v) plane coverage of a particular satellite formation, coordinates of the satellites relative to the position along the reference L2 orbit in the synodic (Earth-Moon rotating) frame are first transformed to the inertial frame and then projected into a plane perpendicular to the line-of-sight to the target. Coordinates in this perpendicular plane are (ξ, η) , and coordinates on the (u, v) plane derived from coordinates in this perpendicular plane are:

$$\begin{aligned} u_i(t) &= \frac{\eta_j - \eta_k}{z\lambda} \\ v_i(t) &= \frac{\xi_j - \xi_k}{z\lambda}, \end{aligned} \tag{9}$$

Here, numerical subscripts j and k indicate that position elements are associated with a particular spacecraft. Numerical subscripts i take values between 1 and $\frac{2j!}{(j-2)!12!}$ because two points in the (u, v) plane are measured for each baseline, and there are as many baselines as pairs of spacecraft in the interferometer formation [11].

Fig. 4a shows a polar plot of the interferometric resolution produced over four days by a formation of four satellites with initial conditions $\Delta x_0 = \pm 30$ meters, $\Delta y_0 = \pm 30$ meters and $\Delta z_0 = \pm 30$ meters at wavelength $\lambda = 780$ nanometers against a 4-meter spherical target orbiting EML4. Similarly, Fig. 4b shows a polar plot of the interferometric resolution

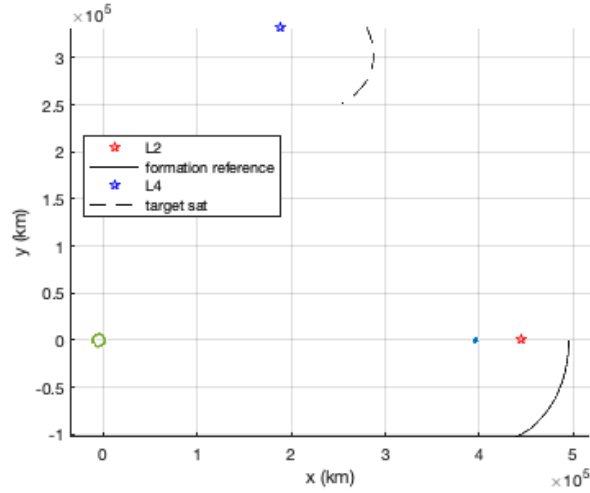


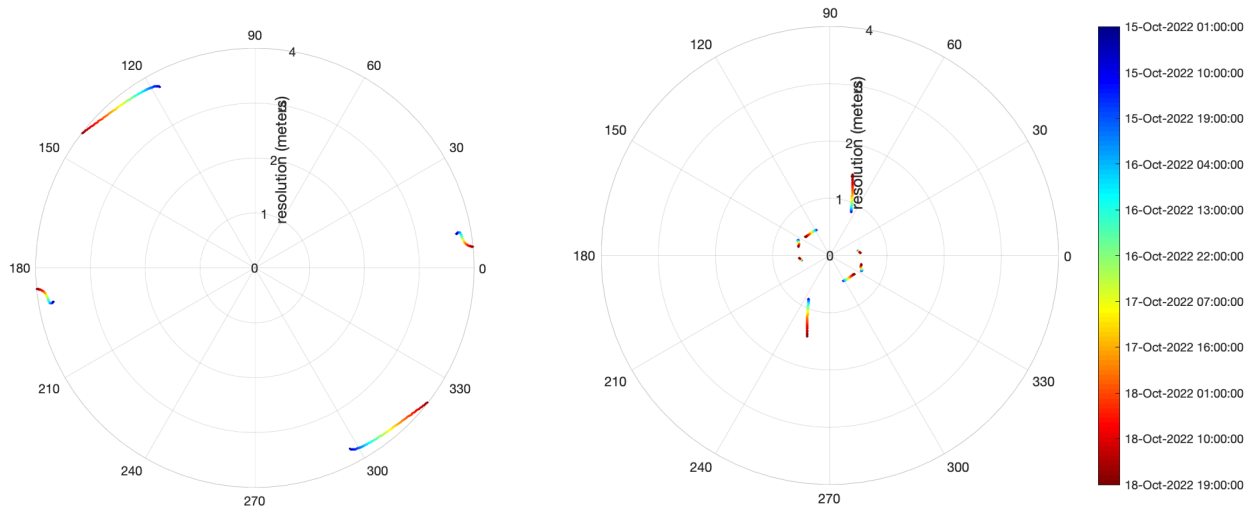
Fig. 3: Four days of motion, shown in the rotating frame, of the formation reference trajectory about Earth-Moon L2 and the target satellite trajectory about Earth-Moon L4. Both trajectories are planar in the rotating Earth-Moon frame. The Earth and Moon are shown in the appropriate positions along the x axis.

produced over four days by a formation of four satellites with initial conditions $\Delta x_0 = \pm 225$ meters, $\Delta y_0 = \pm 225$ meters and $\Delta z_0 = \pm 225$ meters with the same target reflecting the same wavelength of light. Fig. 4c shows a plot of the resolution produced by a formation of eight satellites, and Fig. 4d shows a plot of the resolution produced by a formation of 16 satellites. (See Tab. 1 for further details about the initial conditions of these formations.) We show resolution in meters rather than traditional (u, v) plane coverage in the Fourier domain to improve intuition about these results for the particular tracking custody application addressed in this research. Because the amplitude associated with (u_i, v_i) is equal to the amplitude associated with $(-u_i, -v_i)$, one measurement by a pair of satellites (one baseline) in an interferometer produces two points on the (u, v) plane, resulting in the symmetries apparent in these polar plots [11]. Figs. 4a – 4d demonstrate the improved resolution offered by longer baselines, giving rise to the improved custody result shown in Fig. 5.

As previously discussed, a goal for a formation of satellites performing interferometry in order to produce astrometric observations (unresolved imagery used for precisely measuring the position of a target object rather than the structural details) is to maintain baselines which produce angular resolution very similar to the anticipated target object angular size. The following scalar metric (where P represents a distribution of points) describes the percentage of (u, v) plane points that are covered by the formation but are unnecessary for the desired measurement (where a lower value represents a better result):

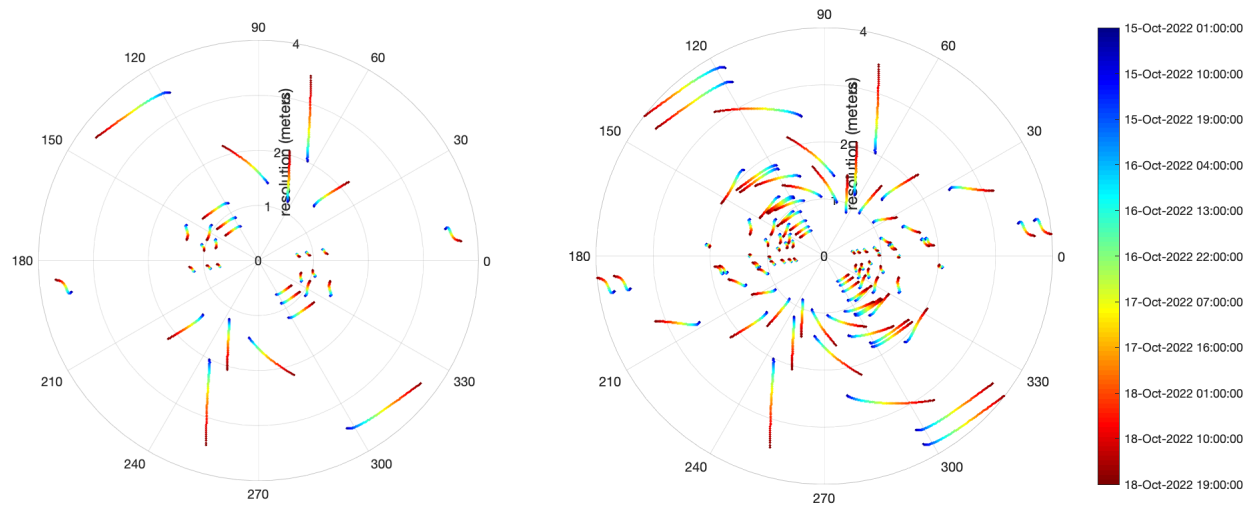
$$c = \int \int |P_{ideal} - P_{formation}| dx dy \quad (10)$$

While P_{ideal} could be defined in many ways, we choose to define P_{ideal} as an annulus with the smaller concentric circle defined by the minimum baseline which will produce a measurement of the target object, which is assumed to be a certain size. The resolution of an interferometer in radians can be calculated as $1.22\lambda/|B|$, and the angular extent of a distant object in radians can be calculated as $\arcsin(\frac{l}{z})$. When the target angular size is smaller than the resolution of the interferometer, the target is not visible to the interferometer. On the other hand, if the target angular size is very much larger than the resolution of the interferometer, we begin to resolve structural details rather than precise position information. In the examples studied for this analysis, we use a spherical target object of diameter four meters. For the interferometer to produce a resolution small enough to detect the target object, a pair of its satellites must create a minimum baseline size of $B_{min} = \frac{1.22\lambda}{\arcsin(\frac{l}{z})}$. Because our goal is not to resolve the structural details of the distant target, we define the diameter of the larger concentric circle of the annulus to be a maximum baseline size defined by $B_{max} = \frac{1.22\lambda}{\arcsin(0.125\frac{l}{z})}$. For our examples we use wavelength $\lambda = 780$ nanometers, which represents the boundary between visible and near-infrared radiation. For distance z , we use an average distance between the reference



(a) Formation of short baselines: 4 spacecraft.

(b) Formation of long baselines: 4 spacecraft.



(c) Formation of medium baselines: 8 spacecraft.

(d) Formation of a variety of baselines: 16 spacecraft.

Fig. 4: Interferometric resolution against a four-meter spherical distant target produced over four days of formation propagation.

EML2 orbit, which is the center of the formation comprising the interferometer, and the target orbiting EML4 for the duration of the measurement collection. The minimum baseline (the inner concentric circle of P_{ideal}), produced as described above for an interferometer orbiting EML2 and observing a 4-meter spherical target orbiting EML4 at 780 nm wavelength, is 98 meters, while the maximum baseline (the outer concentric circle of P_{ideal}) is 783 meters.

In order to compare the scalar metric described above to a quantitative space object tracking custody result, we first check that the baselines are large enough to resolve the target object and cover points in each quadrant of a polar plot of the (u, v) plane. Next we calculate the average resolution for the baselines produced by the given formation for four days. We then use this average resolution as the standard deviation for the production of simulated noisy angular measurements of the target space object orbiting Earth-Moon L4 from the interferometer orbiting Earth-Moon L2. We produce a batch least squares estimate of the target trajectory using hourly simulated noisy angular measurements with batch size four days. (In this case, we assume that this interferometer is used for precise tracking custody of objects in the cislunar regime and not for new object discovery, search, or initial orbit determination.) Thus the interferometer described here must initially be cued by another observer to point at the target object.) We then propagate the estimated and actual target trajectories for one period of the target's EML4 orbit, and we produce a root-sum-squared (RSS) position error at that time. This RSS position error is the metric we use to analyze tracking custody for a given interferometer formation.

Because common impulsive station-keeping methods for collinear Lagrange point orbits involve maneuvers that occur twice per orbit period, control effort for a particular satellite in the formation can be approximated by calculating the difference between the actual and desired distance of the satellite from the reference trajectory after half the reference period has elapsed. The desired distance from the reference trajectory after half the reference period has elapsed is defined as equal to the initial distance of the satellite from the reference trajectory at the start of the simulation. The sum of these differences between actual and desired position for all satellites in the formation is used as a metric for the control effort required for a particular formation.

4. (u, v) PLANE COVERAGE AND TRACKING CUSTODY RESULTS FOR FORMATIONS ABOUT EARTH-MOON LAGRANGE POINT L2

Tab. 1 provides descriptions of four different formations: 1) a formation of four satellites which produce short baselines, 2) a formation of four satellites which produce long baselines, 3) a formation of eight satellites which produce medium baselines, and 4) a formation of 16 satellites with relative motion at a variety of scales, ranging from the small to medium to large scales used in the previous three formations described here.

Fig. 5 shows the (u, v) plane coverage, custody, and control effort results for the formations described in Tab. 1. This figure shows that custody results generally improve as the proposed (u, v) plane coverage metric improves. The formation of four satellites with long baselines is an exception in that its (u, v) plane coverage result is not as favorable as the (u, v) plane coverage result for the medium or variety formation, but its custody result is better than the custody result for either the medium or variety formation. This exception can be explained by the fact that the (u, v) coverage metric we have chosen rewards the sampling of a greater number of points in the (u, v) plane (which can be produced with a greater number of satellites in the formation) as long as these points are within P_{ideal} , while the custody metric rewards longer baselines which produce a smaller average resolution for input to the batch least squares estimator.

Our chosen approximation for control effort demonstrates that formations which produce longer baselines are expected to require greater control effort. In fact, this metric indicates that the medium formation of eight satellites would not require significantly more total control effort than the formation of four satellites with long baselines.

All formations contributing interferometric observations to a cislunar object tracking mission provide dramatically better tracking custody than a single 20 cm telescope.

5. CONCLUSION

This research has shown in simulation the contribution that a formation of satellites performing optical interferometry from an EML2 orbit can bring to tracking custody of a target object orbiting EML4 and provides an approximation of the required control effort for such a formation. All formations are shown to provide orders of magnitude improvement in tracking custody over the observations offered by a single 20 cm telescope. The metrics used in this research

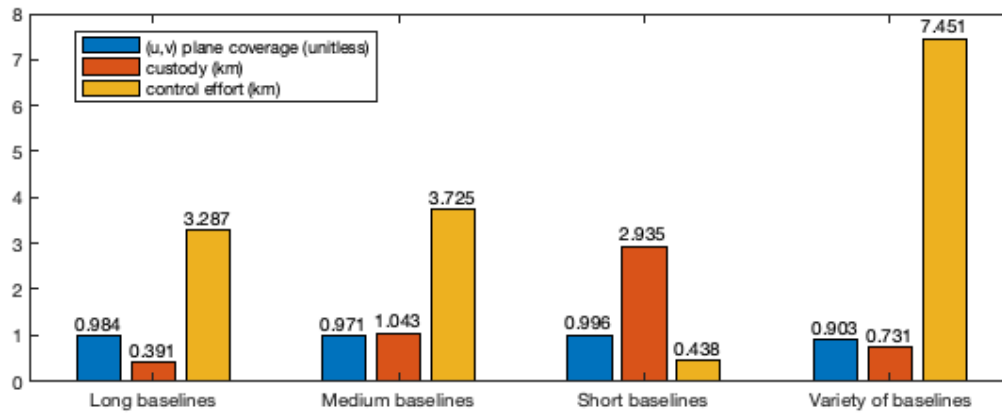


Fig. 5: (u, v) plane coverage, custody, and control effort metric results. Lower values are better for all results. For comparison against the custody results, the RSS position error produced in the same manner from the resolution of a single 20 cm telescope on the nominal EML2 orbit is 756 km.

furnish a method for performing trades, in the early design stage of a flight mission, of the approximate formation control effort, which correlates to formation lifetime, against the formation’s contribution to a cislunar object tracking mission.

Future work on this topic includes studying target objects orbiting Lagrange points other than EML4, as well as consideration of Earth and Moon keep-out zones which would be required for optical and infrared instruments. Future research could also include the development of a control scheme to maintain the desired satellite formation, including an exploration of low-thrust continuous control schemes to minimize control effort. Development of a formation control scheme, regardless of engine type, would also motivate recreating the trajectories in a higher-fidelity dynamics model to understand how acceleration other than Earth and Moon gravitational effects changes the stationkeeping requirement.

Further advice on (u, v) distribution for individual elements in an interferometer is offered in [20]: “The concept of a pseudo-random array is introduced as an array whose large-scale average distribution matches an idealized continuous antenna distribution... Pseudo-random arrays provide a benchmark against which proposed configurations can be compared... The principal advantage of complete coverage is that there are no gaps or holes in the (u, v) coverage, [but] placement of the antennas with a detectable pattern is likely to worsen the PSF... The formulas in this paper can aid in making the tradeoff between the size and number of antennas during the initial conceptual design of an interferometer array... The optimal configuration will depend upon the science goals for an array but the concepts and results derived here should make it easier to investigate the many options.” Future work could include establishing comparisons between the (u, v) plane coverage that is produced by satellites in a formation about an Earth-Moon Lagrange point to a uniform random distribution of points in the (u, v) plane.

6. REFERENCES

- [1] S. Chakravorty, P.T. Kabamba, and D.C. Hyland. Modeling of image formation in multi-spacecraft interferometric imaging systems. In *AIAA Space Conference*, number 5895, San Diego, California, September 2004.
- [2] Cislunar Technology Strategy Interagency Working Group of the National Science & Technology Council. National cislunar science & technology strategy, November 2022.
- [3] E.E. Fowler and D.A. Paley. Observability metrics for space-based cislunar domain awareness. *Journal of the Astronautical Sciences*, April 2023.
- [4] G. Gomez, J. Llibre, R. Martinez, and C. Simo. *Dynamics and Mission Design Near Libration Points, Fundamentals: The Case of Collinear Libration Points*, volume 2 of *World Scientific Monograph Series in Mathematics*. World Scientific Publishing, 4 2001.
- [5] D. J. Grebow. Generating periodic orbits in the circular restricted three-body problem with applications to lunar south pole coverage. Master’s thesis, Purdue University, West Lafayette, IN, May 2006.

- [6] N. H. Hamilton. Formation flying satellite control around the 12 sun-earth libration point. Master's thesis, The School of Engineering and Applied Science of the George Washington University, Washington, DC, September 2001.
- [7] K. H. Howell and L. D. Millard. Control of satellite imaging formations in multi-body regimes. *Acta Astronautica*, 64:554–570, 2009.
- [8] I.I. Hussein, D.J. Scheeres, and D.C. Hyland. Control of a satellite formation for imaging applications. In *American Control Conference*, July 2003.
- [9] D.C. Hyland. Interferometric imaging concepts with reduced formation-keeping constraints. In *AIAA Space Conference*, Albuquerque, New Mexico, August 2001.
- [10] W. S. Koon, M. W. Lo, J. E. Marsden, and S. D. Ross. *Dynamical Systems, the Three-Body Problem and Space Mission Design*. Springer, 2007.
- [11] L. D. Millard. *Control of Satellite Imaging Arrays in Multi-Body Regimes*. PhD thesis, Purdue University, West Lafayette, IN, May 2008.
- [12] L.D. Millard and K.C. Howell. Control of interferometric spacecraft arrays for (u, v) plane coverage in multi-body regimes. *Journal of Astronautical Sciences*, 56(1), January—March 2008.
- [13] F. Millour. Interferometry concepts. *EAS publication series*, 69-70, 2015.
- [14] D. Mourard. Optical long baseline interferometry: Examples from vega/chara. *New Concepts in Imaging: Optical and Statistical Models*, 59:25–36, 2013.
- [15] S. Parr, S. Wirwille, B. MacDonald, E. Fowler, B. Schmachtenberger, B. Bauer, E. Klatt, R. Mitch, E. Birrane, and S. Heiner. Cislunar security national technical vision. Technical report, Johns Hopkins Applied Physics Laboratory, Laurel, MD, November 2022.
- [16] A. E. Roy. *Orbital Motion*. Taylor & Francis Group, 4th edition, 2005.
- [17] A. Segerman and M. Zedd. Investigations of spacecraft orbits around the 12 sun-earth libration point. Technical Report NRL/MR/8233–05-8897, United States Naval Research Laboratory, 4555 Overlook Avenue SW, Washington, DC 20375-5320, July 2005.
- [18] J. Wachs, J. Lee, R. Linfield, J. Kommers, and W. Cash. Spectrally resolved synthetic aperture imaging interferometer. Technical Report 17-NIAC18B-0145, Ball Aerospace, January 2019.
- [19] D. Woody. Alma configurations with complete uv coverage. Technical Report 270, California Institute of Technology Owens Valley Radio Observatory, Big Pine, CA, August 1999.
- [20] D. Woody. Radio interferometer array point spread functions. Technical Report 389, California Institute of Technology Owens Valley Radio Observatory, Big Pine, CA, August 2001.
- [21] F. Zernike. The concept of degree of coherence and its application to optical problems. *Physica*, 5(38):785–795, August 1938.

APPENDIX A

Table 1: Initial conditions for four formations.

Formation Description	Initial Conditions (m)
Short baselines (4 satellites)	$\Delta x_0 = 30, \Delta y_0 = 30, \Delta z_0 = 30$ $\Delta x_0 = -30, \Delta y_0 = -30, \Delta z_0 = -30$ $\Delta x_0 = 30, \Delta y_0 = 30, \Delta z_0 = -30$ $\Delta x_0 = -30, \Delta y_0 = -30, \Delta z_0 = 30$
Long baselines (4 satellites)	$\Delta x_0 = 225, \Delta y_0 = 225, \Delta z_0 = 225$ $\Delta x_0 = -225, \Delta y_0 = -225, \Delta z_0 = -225$ $\Delta x_0 = 225, \Delta y_0 = 225, \Delta z_0 = -225$ $\Delta x_0 = -225, \Delta y_0 = -225, \Delta z_0 = 225$
Medium baselines (8 satellites)	$\Delta x_0 = 95, \Delta y_0 = 95, \Delta z_0 = 95$ $\Delta x_0 = -95, \Delta y_0 = -95, \Delta z_0 = -95$ $\Delta x_0 = 95, \Delta y_0 = 95, \Delta z_0 = -95$ $\Delta x_0 = -95, \Delta y_0 = -95, \Delta z_0 = 95$ $\Delta x_0 = 160, \Delta y_0 = 160, \Delta z_0 = 160$ $\Delta x_0 = -160, \Delta y_0 = -160, \Delta z_0 = -160$ $\Delta x_0 = 160, \Delta y_0 = 160, \Delta z_0 = -160$ $\Delta x_0 = -160, \Delta y_0 = -160, \Delta z_0 = 160$
Variety baselines (16 satellites)	$\Delta x_0 = 30, \Delta y_0 = 30, \Delta z_0 = 30$ $\Delta x_0 = -30, \Delta y_0 = -30, \Delta z_0 = -30$ $\Delta x_0 = 30, \Delta y_0 = 30, \Delta z_0 = -30$ $\Delta x_0 = -30, \Delta y_0 = -30, \Delta z_0 = 30$ $\Delta x_0 = 95, \Delta y_0 = 95, \Delta z_0 = 95$ $\Delta x_0 = -95, \Delta y_0 = -95, \Delta z_0 = -95$ $\Delta x_0 = 95, \Delta y_0 = 95, \Delta z_0 = -95$ $\Delta x_0 = -95, \Delta y_0 = -95, \Delta z_0 = 95$ $\Delta x_0 = 160, \Delta y_0 = 160, \Delta z_0 = 160$ $\Delta x_0 = -160, \Delta y_0 = -160, \Delta z_0 = -160$ $\Delta x_0 = 160, \Delta y_0 = 160, \Delta z_0 = -160$ $\Delta x_0 = -160, \Delta y_0 = -160, \Delta z_0 = 160$ $\Delta x_0 = 225, \Delta y_0 = 225, \Delta z_0 = 225$ $\Delta x_0 = -225, \Delta y_0 = -225, \Delta z_0 = -225$ $\Delta x_0 = 225, \Delta y_0 = 225, \Delta z_0 = -225$ $\Delta x_0 = -225, \Delta y_0 = -225, \Delta z_0 = 225$